Hypoxia in the upper reaches of the Pearl River Estuary and its maintenance mechanisms: A synthesis based on multiple year observations during 2000–2008

Biyan He [a,b], Minhan Dai [a,*], Weidong Zhai [a], Xianghui Guo [a], Lifang Wang [a]

[a] State Key Laboratory of Marine Environmental Science, Xiamen University, Xiamen 361005, China
[b] School of Bioengineering, Jimei University, Xiamen 361021, China

ARTICLE INFO

ABSTRACT

Based on our multiple year observations during 2000–2008 in the Pearl River Estuary, this study sought to synthesize the long-term pattern of hypoxia and its relationship to organic carbon and nutrient loading in this important world major estuary under significant human impacts. We confirmed previously observed year-round low dissolved oxygen (DO) of <63 μmol kg^{-1} reaching the threshold of hypoxia in the upper reaches of the Pearl River Estuary, extended from the Guangzhou Channel to downstream of the Humen Outlet, in the surface water, covering a water body of ~75 km length. The surface DO concentration had a significantly negative correlation with dissolved and particulate organic carbon, and NH_4^+ concentrations. Both aerobic respiration and nitrification highly varied spatially in the water column. The highest rates of respiration and nitrification were observed in the Guangzhou Channel, which decreased downstream along with organic carbon and NH_4^+ concentrations. Seasonally, the highest rates of total oxygen consumption upon normalization to the substrate (TOC, total organic carbon; and NH_4^+) were observed in summer, suggesting that both the substrate availability and water temperature were major factors controlling the oxygen consumption rates. Oxygen mass balance calculations showed that in summer, the oxygen consumption rate in the water column by aerobic respiration (21.3×10^6 mol O_2 d^{-1}) and nitrification (14.5×10^6 mol O_2 d^{-1}) was almost balanced by the reaeration (32.6×10^6 mol O_2 d^{-1}) and net advective complement (2.3×10^6 mol O_2 d^{-1}). The contributions of other processes (e.g., sediment oxygen consumption and photosynthesis) appeared to be minor. We estimated that the on-site biogenically produced organic matter, or autochthonous organic material, contributed only 13% ± 10% of the TOC being respired in the hypoxic area, suggesting that the allochthonous organic material, primarily derived from sewage discharge, dominated aerobic respiration and the associated oxygen consumption. Meanwhile, NH_4^+ which was clearly reflective of sewage loadings (if not all) dominated the nitrification process and the associated oxygen consumption. Taken together, the hypoxia in the studied area was profoundly anthropogenic and this conclusion should have many implications towards regional environmental management.

© 2014 Elsevier B.V. All rights reserved.

1. Introduction

Hypoxic waters, typically defined when dissolved oxygen (DO) concentration falls below 2–3 mg L^{-1} (or 63–95 μmol O_2 kg^{-1}), have become one of the most pressing worldwide environmental problems in many estuaries and coastal areas (Diaz and Rosenberg, 2008). The formation, development and maintenance of hypoxia usually depend on both physical and biogeochemical conditions of a particular water body. Physical processes such as stratification, circulation pattern, and the flushing rate influence the horizontal and vertical transport of DO (Lin et al., 2008; Rabouille et al., 2008). Biogeochemical processes include the consumption (e.g. respiration of organic matter and nitrification) or production of DO (e.g. photosynthesis).

The majority of the studies on hypoxia have focused on the inner shelf regimes where anthropogenic nutrients drive excess algal biomass production, the subsequent accumulation of which in the bottom water fuels microbial-mediated organic matter decomposition. This consumes large amounts of oxygen and, if the water column was stratified with limited DO replenishment from the surface, DO in the bottom water could become depleted. This mechanism has explained the oxygen depletion in many shelf systems, e.g. the Long Island Sound, the northern Gulf of Mexico and Chesapeake Bay (Hagy et al., 2004; Justic et al., 2002; Lee and Lwiza, 2008; Scavia et al., 2003; Turner et al., 2005), where the linkage between anthropogenic nutrient loads and hypoxia is well documented.

* Corresponding author.
 E-mail address: mdai@xmu.edu.cn (M. Dai).

Another setting of hypoxia is increasingly recognized to occur in well-mixed estuaries (Verity et al., 2006), mostly in highly impacted upper estuaries such as the Pearl River Estuary (PRE), Scheldt Estuary and Seine Estuary (Dai et al., 2006; Frankignoulle et al., 1996; Garnier et al., 2001). In this type of settings, high loads of allochthonous organic matter and nutrients (especially NH_4^+) from wastewater discharge might directly stimulate microbial respiration and nitrification and result in oxygen depletion in the water column, often only in the confined upper estuary. However, the mechanistic understanding and quantification of the contribution of individual processes to the overall oxygen depletion in these well-mixed estuaries are not well demonstrated.

The Pearl River is the largest river in southern China. With the rapid economic development and urbanization in the Pearl River Delta, human activity has seriously affected the regional environment during the past few decades. A very low DO concentration was observed in water columns in the upper reaches of the PRE, or upstream of the Humen Outlet, which have been attributed to organic matter respiration and nitrification (Dai et al., 2006, 2008a; He et al., 2010b). However, the origin of organic matter in supporting microbial respiration has not yet been characterized. Neither have the relative contributions of microbial respiration and nitrification to the oxygen consumption been well quantified. This problem is significant because it is essential in guiding environment management policies. In this study, we synthesized observations from 2000 to 2008 based on multiple cruises in order to further define the oxygen depletion zone and to examine the seasonal and interannual variations in DO conditions in the upper reaches of the PRE. Multiple physical and hydrochemical parameters were simultaneously determined to evaluate the effects of the alterations in physical conditions, nutrient and organic carbon loads on hypoxic conditions. On-deck oxygen metabolic incubations were carried out to further elucidate the mechanisms controlling oxygen depletion. Finally, a mass balance model was adopted to quantify the relative contribution of individual processes to the formation and the maintenance of this oxygen depletion zone, and to evaluate the role of allochthonous versus autochthonous organic matter in supporting microbial respiration throughout the hypoxic region.

2. Materials and methods

2.1. Study area

The Pearl River is one of the world's 20 largest rivers, with an annual river discharge of ~330 × 10⁸ m³, 80% of which is delivered during the wet season from April to September. The PRE consists of three sub-estuaries, namely Modaomen, Huangmaohai and Lingdingyang Bay. Among them, Lingdingyang Bay (traditionally regarded as the PRE) is the largest, and receives ~53% of the river runoff via the northern four outlets, i.e. Humen, Jiaomen, Hengmen, and Hongqimen (Dai et al., 2014 and references therein).

Our study focused on the upper reaches of the PRE; the upstream of Lingdingyang Bay, stretching from the Humen Outlet upward to the suburbs of Guangzhou with a total length of ~75 km; and four segments, the Guangzhou, Huangpu, Shiziyang and Humen Channels (Fig. 1). The Guangzhou Channel is ~32 km long with an average width of ~525 m and an average depth of ~5.0 m (Guangzhou Record, http://www.gzsdfz.org.cn). It runs across the city of Guangzhou, the most urbanized and heavily impacted district in southern China, with ~12.7 million inhabitants (http://www.gzatats.gov.cn/rkpc/) and numerous industrial and agricultural settings. The Huangpu to Humen Channel is ~45 km long with an average width of ~2.2 km and an average water depth of ~6.6 m (http://www.gzsdfz.org.cn). It receives inflows from the Guangzhou Channel and the East River, and two cities, Panyu and Dongguan, are in the area, where agriculture and countryside industry are well developed and, thereby, the anthropogenic loads have dramatically increased in the last few decades (Table 1). As a consequence of high organic carbon and nutrient loads, the aquatic environments of

the upper reaches of the PRE have deteriorated in recent years. A serious year-round oxygen depletion in the water column is noted in this area (Dai et al., 2006, 2008a; Zhai et al., 2005).

2.2. Data sources and new observations

This study synthesized the historical data from July 2000, May–June 2001, November 2002, February 2004, January 2005, August 2005, March 2006, and the new observations in April 2007, and August 2008. The major parameters observed and the detailed data sources are shown in Table 2. These cruises covered four seasons, representing the cold and dry season with low water flow, the warm and flood season with high water flow and the transitional seasons with medium flow.

Sampling was carried out on board R/V Yanping II during 2000–2004, and on another vessel, the Yue Dongguang 00589, during 2005–2008. Underway pumping was performed for continuous measurements of temperature, salinity and DO. The details of our underway pumping system were described previously (Dai et al., 2006, 2009; Zhai et al., 2005; Guo et al., 2009). Discrete underway sampling was also conducted for salinity and DO measurements using this system guided by the salinity gradient within the estuarine mixing zone and by distance where no significant salinity gradient occurred upstream of the Humen Outlet. Surface samples for nitrogenous nutrients (NH_4^+, NO_2^-, NO_3^-) and dissolved organic carbon (DOC) were collected with another pumping system equipped with a FloJet® pump and an on-line acid-cleaned cartridge filter (He et al., 2010b).

In addition to the surface water sampling, water column samples for DO, DOC, particulate organic carbon (POC), total suspended matter (TSM), chlorophyll a (Chl-a), NH_4^+, NO_2^-, and NO_3^- were collected using a SEACAT CTD (SBE19 Sea-Bird Co.) rosette system equipped with Niskin or Go-Flo bottles. Sub-samples for DOC, POC, Chl-a, TSM and nutrients are collected following the procedures described previously (Dai et al., 2006; He et al., 2010b).

At selected stations, we used incubations to determine the O_2 production from the primary production, and O_2 consumption from microbial respiration and nitrification. These stations are numbered in Fig. 1.

2.3. Analysis

2.3.1. Underway measurements of surface temperature, salinity, DO and meteorological data

Temperature and salinity (conductivity) of the surface water were continuously measured using a SEACAT thermosalinograph system (CTD; SBE21, Sea-Bird Co.) for the first two cruises, and using a Yellow Spring Instrument multi-parameter meter (YSI® 6600) for the other cruises (see details in Dai et al., 2006; Zhai et al., 2005). Surface water DO was monitored continuously using a pre-calibrated DO probe assembled on the YSI® equipped to an underway pumping system (Zhai et al., 2005). Our CTD sensors were calibrated at the National Center of Ocean Standards and Metrology of China every year. Temperature and salinity probes of YSI were calibrated with CTD sensors just prior to the cruises. The DO probe of YSI was calibrated against water saturated air. Winkler DO samples including different levels of DO were occasionally taken for ground truth of the probe data. Meteorological data including wind speed were collected with an onboard weather station set at ~10 m above the sea surface.

2.3.2. DO, Chl-a, nutrients, TSM, POC and DOC of the discrete samples

The DO concentration in discrete samples was determined on board following the classic Winkler procedure. A small quantity of NaN_3 was added during subsample fixation to remove possible interference from nitrites (Wong, 2012). Based on replicated measurements of the NaS_2O_3 titration reagent concentration, the uncertainty of our DO data was estimated to be at a satisfactory level of <0.5%. The DO saturation (DO%) was calculated from the field-measured DO concentration
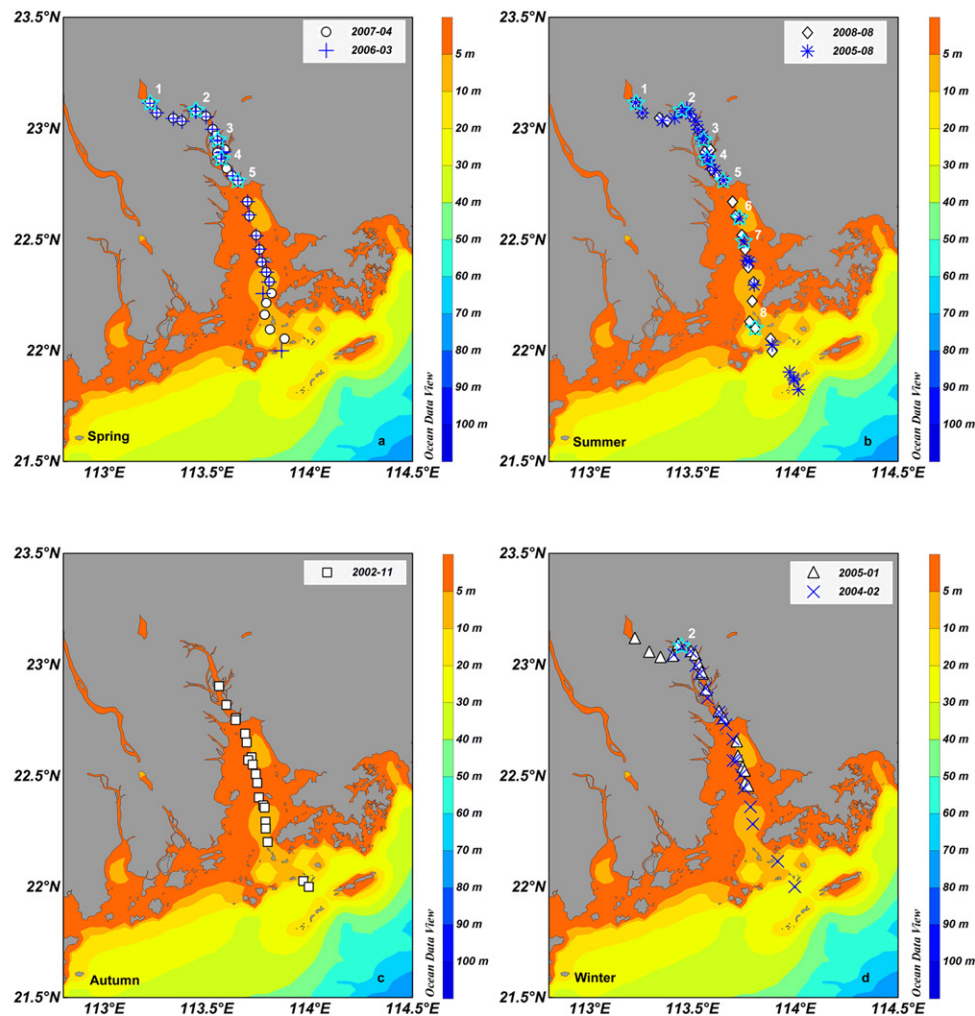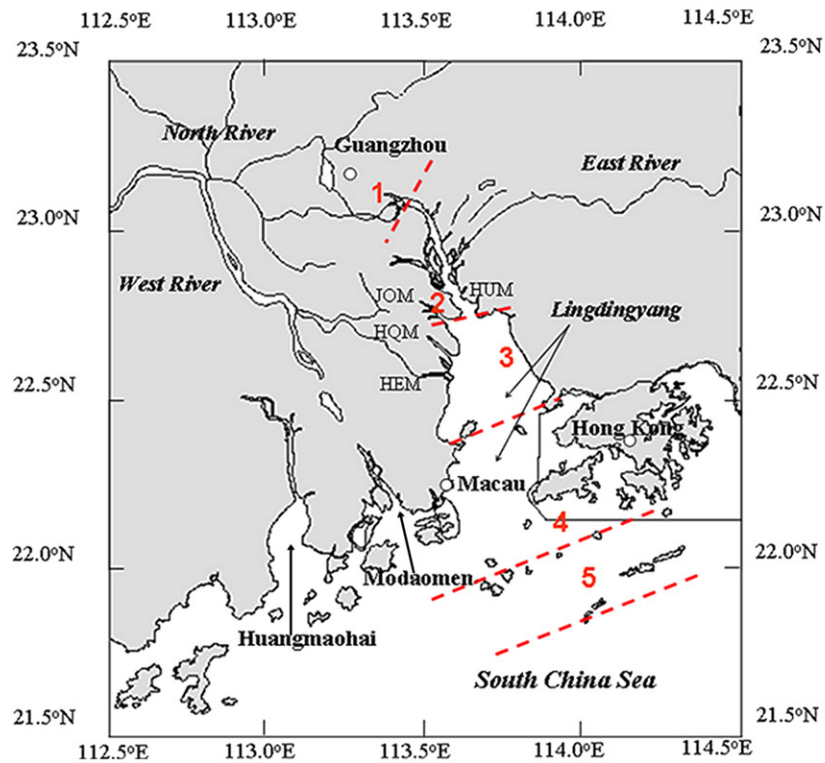
Fig. 1. Map of the Pearl River Estuary and the sampling sites (a, b, c and d) in the seven cruises during 2000–2008. HUM, JOM, HQM and HEM represent Humen, Jiaomen, Hongqimen, and Hengmen, which are the eastern four outlets of the Pearl River Estuary. The three sub-estuaries, Lingdingyang, Modaomen and Huangmaohai, are also indicated. Open stars in panels a, b and d show the incubation stations: in April 2007, the total oxygen consumption incubations were carried out at Stations 1, 2, and 5, while nitrification incubations were carried out at Stations 1–5 (open stars in panel a). In August 2008 total oxygen consumption incubations were carried out at Stations 1–8, while nitrification incubations were carried out at Stations 1–5 (b); in February 2004, August 2005 and March 2006, both total oxygen consumption and nitrification incubations were carried out only in Station 2. For ease of discussion, we divided the Pearl River Estuary into five zones: 1 and 2 — upper reaches; 3 — middle estuary (mixing-dominated zone); 4 — lower estuary; 5 — inner shelf. Stations 1–2 were located in the Guangzhou Channel, Stations 2–3 in the Huangpu Channel, Stations 3–4 in the Shiziyang Channel, and 4–5 in the Humen Channel.

Table 1
Wastewater discharge from Guangdong Province and their treatment rates between 2000 and 2008. Data are from the Environmental Status Bulletins of Guangdong Province, China (http://www.gdepb.gov.cn/zwxx/tjsj/index.html).

	2000	2001	2002	2003	2004	2005	2006	2007	2008
Total wastewater discharge (10^8 tons)	44.8	51.1	49.0	54.6	54.2	63.8	65.5	69.1	67.7
Industrial effluent (10^8 tons)	11.4	11.3	14.6	14.9	16.5	23.2	23.5	24.6	21.3
Domestic sewage (10^8 tons)	33.4	39.9	34.4	39.8	37.7	40.7	42.0	44.5	46.4
Total chemical oxygen demand (COD) emission in wastewater (10^4 tons)	95.1	110.3	95.2	98.2	92.7	105.8	104.9	101.7	96.4
Industrial COD (10^4 tons)	28.2	21.6	20.7	21.1	24.9	29.2	29.4	28.1	21.1
Domestic COD (10^4 tons)	67	88.7	74.5	77.1	67.8	76.7	75.5	73.7	75.3
Total ammonium discharge (10^4 tons)	–	9.0	8.5	9.3	8.7	10	9.3	12	12.2
Industrial ammonium (10^4 tons)	–	0.9	1.0	0.8	0.9	0.9	0.7	1.1	1.0
Domestic ammonium (10^4 tons)	–	8.1	7.6	8.5	7.7	9.1	8.6	10.9	11.2
Rate of industrial wastewater treatment (%)	81.8	84.1	78.3	82.9	83.9	83.9	84.9	86.1	89.7
Overall rate of domestic sewage treatment (%)	17.2	16.6	21.2	24.7	35.7	40.2	45.3	50.2	55.9

divided by DO concentration at equilibrium with the atmosphere as per the Benson and Krause (1984) equation and local air pressure.

Chl-a was determined using a Turner fluorometer after extraction of the membrane samples with 90% acetone (Parsons et al., 1984). Calibrations were performed using Sigma Chl-a standard. Nutrients were analyzed following our reported methods (Dai et al., 2006, 2008a). Briefly, NH_4^+ was analyzed on deck with the indophenol blue spectrophotometric method; NO_2^- and NO_3^- were determined using classic colorimetric methods with a Technicon AA3 Auto-analyzer (Bran-Lube) in a land-based laboratory in Xiamen University. POC was analyzed on a Perkin Elmer 2400IICHS/O elemental analyzer after removal of carbonate with HCl fumes for 24 h (see details in Zhou et al., 2013), and DOC concentrations were determined using high-temperature catalytic oxidation techniques with a Shimadzu TOC-V CPH TOC analyzer.

2.4. On-deck incubation experiments

2.4.1. Total oxygen consumption rates

Total oxygen consumption rates were determined at Stations 1–8 (see Fig. 1 for locations) by monitoring temporal changes in O_2 concentration of unfiltered water incubated in 300 mL BOD bottles in the dark

(He et al., 2010b). Briefly, surface water from a depth of ~1 m and bottom water from ~2 m above the sediment surface were collected with Go-Flo bottles and filled into BOD bottles and incubated in the dark at ambient temperature controlled by the flowing surface water. Poisoned control treatments were also established with 0.1% (v/v) saturated $HgCl_2$ added at the initial time point of the experiment. Sub-samples were taken every 2–24 h according to the initial DO concentration (low initial DO with short incubation time) during the incubation. Duplicate sub-samples were taken and determined. The oxygen consumption rates were calculated from the DO decrease during incubation. In this study, total oxygen consumption was partitioned into nitrification and microbial respiration.
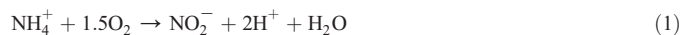
2.4.2. Nitrification and microbial respiration rates

Nitrification rates were measured using an inhibitor technique as described in Dai et al. (2008a). Briefly, water samples were homogenized in a 20 L pre-cleaned polyethylene container, and then dispensed into 4 L narrow neck amber glass bottles. 100 mg L^{-1} of allylthiourea (ATU) was added into one incubation bottle to inhibit the oxidation of ammonia (NH_3) to nitrite (NO_2^-). At the same time, 10 mg L^{-1} of $NaClO_3$ was added into another incubation bottle to inhibit the

Table 2
Data sources for this study.

Season	Cruises	Parameters	Data sources
Spring	March-2006	DO	Dai et al. (2008a) and Guo et al. (2009)
		TOC	This study
		NH_4^+, NO_3^-	Dai et al. (2008a)
	April-2007	DO	Guo et al. (2009) and He et al. (2010b)
		TOC	This study
		NH_4^+, NO_3^-	He et al. (2010b)
		Chl-a	He et al. (2010b)
		Respiration rate	This study
		Nitrification rate	This study
		Photosynthesis rate	This study
Summer	July-2000	DO	Zhai et al. (2005)
	June-2001	DO	Zhai et al. (2005)
	August-2005	DO	Dai et al. (2008a) and Guo et al. (2009)
		TOC	This study
		NH_4^+, NO_3^-	Dai et al. (2008a)
	August-2008	DO	This study
		TOC	This study
		NH_4^+, NO_3^-	This study
		Chl-a	This study
		Respiration rate	This study
		Nitrification rate	This study
		Photosynthesis rate	This study
Autumn	November-2002	DO	Guo et al. (2009)
		TOC	This study
Winter	February-2004	DO	Dai et al. (2006) and Guo et al. (2009)
		TOC	This study
		NH_4^+, NO_3^-	Dai et al. (2006)
	January-2005	DO	Dai et al. (2008a) and Guo et al. (2009)
		NH_4^+, NO_3^-	Dai et al. (2008a)

oxidation of NO_2^- to nitrate (NO_3^-). Nitrification rates were estimated from the evolution of NO_2^- concentrations in incubation bottles during the incubation. The nitrification oxygen consumption rates were calculated using a stoichiometric approach based on the simplified nitrification reactions (1) and (2).

$$NH_4^+ + 1.5O_2 \rightarrow NO_2^- + 2H^+ + H_2O \tag{1}$$

$$NO_2^- + 0.5O_2 \rightarrow NO_3^- \tag{2}$$

The microbial respiration rate was calculated as the difference obtained after subtracting the nitrification induced oxygen consumption rate from the total oxygen consumption rate.

2.4.3. Photosynthetic O_2 production rates

The optimum primary productivity (P_{max}) was estimated from the surface Chl-a content (Platt and Sathyendranath, 1993; Ryther and Yentsch, 1957):

$$P_{max} = C_S \times Q \times D \tag{3}$$

where C_S is the surface water Chl-a concentration (mg m^{-3}), Q is the assimilation coefficient (mg C (mg Chl-a)$^{-1}$ h^{-1}), and D is the daily irradiation time (assuming 12 h d^{-1} in winter and 13 h d^{-1} in summer). We adopted the average value of Q as 4.8 mg C (mg Chl-a)$^{-1}$ h^{-1} in the upper reaches and middle estuary, and 9.2 mg C (mg Chl-a)$^{-1}$ h^{-1} in the lower estuary and inner shelf for median P_{max} estimation as suggested in previous studies (Cai et al., 2002; Huang et al., 2005). This estimated P_{max} was comparable to the traditional light–dark bottle oxygen incubation results measured in surface water in two stations, which were 176 mmol O_2 m^{-3} d^{-1} (estimated value) vs. 132 mmol O_2 m^{-3} d^{-1} (measured value) for Station 2, and 59 mmol O_2 m^{-3} d^{-1} (estimated value) vs 60 mmol O_2 m^{-3} d^{-1} (measured value) for Station 3. We also used Q + 1σ and Q − 1σ to estimate the upper limit and the lower limit of P_{max} in order to make the estimation more reasonable.

Primary productivity at a certain depth (Z m) was formulated as a function of available light and the P_{max}:

$$P_z = P_{max} \times I_z/I_0 \tag{4}$$

$$I_z = I_0 \times e^{-\kappa z}. \tag{5}$$

On substituting Eq. (5) into Eq. (4), we get

$$P_z = P_{max} \times e^{-\kappa z} \tag{6}$$

where Z is the water depth (m), P_z is the primary productivity at Z depth, I_z is the irradiance at Z depth, I_0 is the irradiance at the surface, and κ is the mean downwelling attenuation coefficient. Water column primary productivity was integrated over the water column to the euphotic zone (the 1% surface light depth). A previous study shows that the mean downwelling attenuation coefficient is 3–4 m^{-1} near the four outlets, decreases to 1–2 m^{-1} in the middle estuary and to <0.9 m^{-1} in the lower estuary (Yin et al., 2004). The euphotic zone was 1–1.5 m near the four outlets, increased to 2–4 m in the middle estuary and to 4–8 m in the lower estuary. Vertically integrated rates of photosynthetic O_2 production (P_i) were calculated by integrating the primary production assuming a mean photosynthetic quotient ($\Delta O_2/\Delta C$) of 1.25 (Ryther, 1956; Oviatt et al., 1986; Williams and Robertson, 1991).

It should be pointed out that this P_i was a first order estimation, which was subject to uncertainties, including spatial variations of Q, the fluctuation of light, and the variation of photosynthetic quotient. Based on the limited field measurement of Q in this studied area, the spatial variation (1σ) of Q is ±3.5 mg C (mg Chl-a)$^{-1}$ h^{-1} in the upper and middle estuaries, and ±5.0 mg C (mg Chl-a)$^{-1}$ h^{-1} in the lower estuary (Cai et al., 2002; Huang et al., 2005). The fluctuation of solar radiation was ~37% in summer (Hong Kong Observatory, http://www.hko.gov.hk). The typical variation of photosynthetic quotient was within 20–23% (Oviatt et al., 1986; Williams and Robertson, 1991). The composite uncertainty would be at most ~85% and 70% in the P_i estimation respectively in the upper and lower estuaries.

2.5. Air–water O_2 flux estimation

The air–water O_2 flux (F, mmol m^{-2} d^{-1}) was estimated based on the following equation (Skjelvan et al., 2001):

$$F = -k \times ([O_2]_m - [O_2]_s) \tag{7}$$

where $[O_2]_m$ was the measured oxygen content in the surface water and $[O_2]_s$ was the corresponding saturation concentration calculated following the equation of Benson and Krause (1984). A positive value represented the net O_2 influx to the water body and a negative value referred to the net O_2 efflux from the water body to the atmosphere. k is the gas transfer velocity of O_2, which was estimated based on the Wanninkhof (1992) empirical function with wind speed:

$$k = 0.31 \times u^2 \times (Sc/Sc')^{-1/2} \tag{8}$$

where u was the field-measured wind speed in m s^{-1} at a 10 m height; Sc and Sc' were Schmidt numbers. Sc was calculated using the algorithm proposed by Wanninkhof (1992). In our study, S < 20 was treated as freshwater, while S > 20 was treated as seawater. Sc' is the Schmidt number of O_2 at 20 °C (Wanninkhof, 1992). In the PRE, the mean wind speeds were 4.3 ± 1.8 m s^{-1} for the August 2008 survey, 4.5 ± 2.4 m s^{-1} for the April 2007 survey, 4.4 ± 1.0 m s^{-1} for the November 2002 survey, and 4.3 ± 3.1 m s^{-1} for the February 2004 survey. These average wind speeds were used for the calculation of the seasonal water–air O_2 fluxes.

3. Results

3.1. Hydrological settings

Freshwater discharge rates of the Pearl River showed significant seasonal variations. The highest discharge rate, during our cruises, was ~13,700 m^3 s^{-1} in August 2008, which was ~6 times that in the dry season (~2200 m^3 s^{-1} in January 2005 and ~2300 m^3 s^{-1} in February 2004). The inter-annual variation of freshwater discharge was much more significant in the wet season than in the dry season. In the vicinity of the Humen Outlet, salinity was 0 in August 2008 compared with ~15 in February 2004 and January 2005 (Fig. 2a), reflecting the greatly different discharge rates between the wet and dry seasons. The freshwater end-member was located at the vicinity of Humen in August 2008, but saline water (S > 0.5) intruded upon the suburbs of Guangzhou (~70 km upstream of Humen) in January 2005. The surface temperature of the surveyed area ranged from 23.2 to 25.5 °C (in spring), 27.2 to 30.9 °C (in summer), 21.2 to 23.9 °C (in autumn) and 14.3 to 17.4 °C (in winter).

3.2. Spatial distribution and seasonal variation of surface DO

Hypoxia indeed existed in the surface water in the upper reaches of the PRE, or upstream Humen throughout the year (Fig. 2c). This oxygen depleted zone in most time of the year extended from Humen to the suburbs of Guangzhou, covering ~75 km of the water body, with the lowest surface DO concentration of 2–9 μmol O_2 kg^{-1} near Guangzhou. Downstream the Humen Outlet, surface DO concentration increased gradually with salinity, almost reaching saturation or supersaturation in the lower estuary. Seasonally, the most severe oxygen depletion was observed in spring, followed by that in summer and winter. In spring, surface DO was <63 μmol O_2 kg^{-1} in the entire upstream of
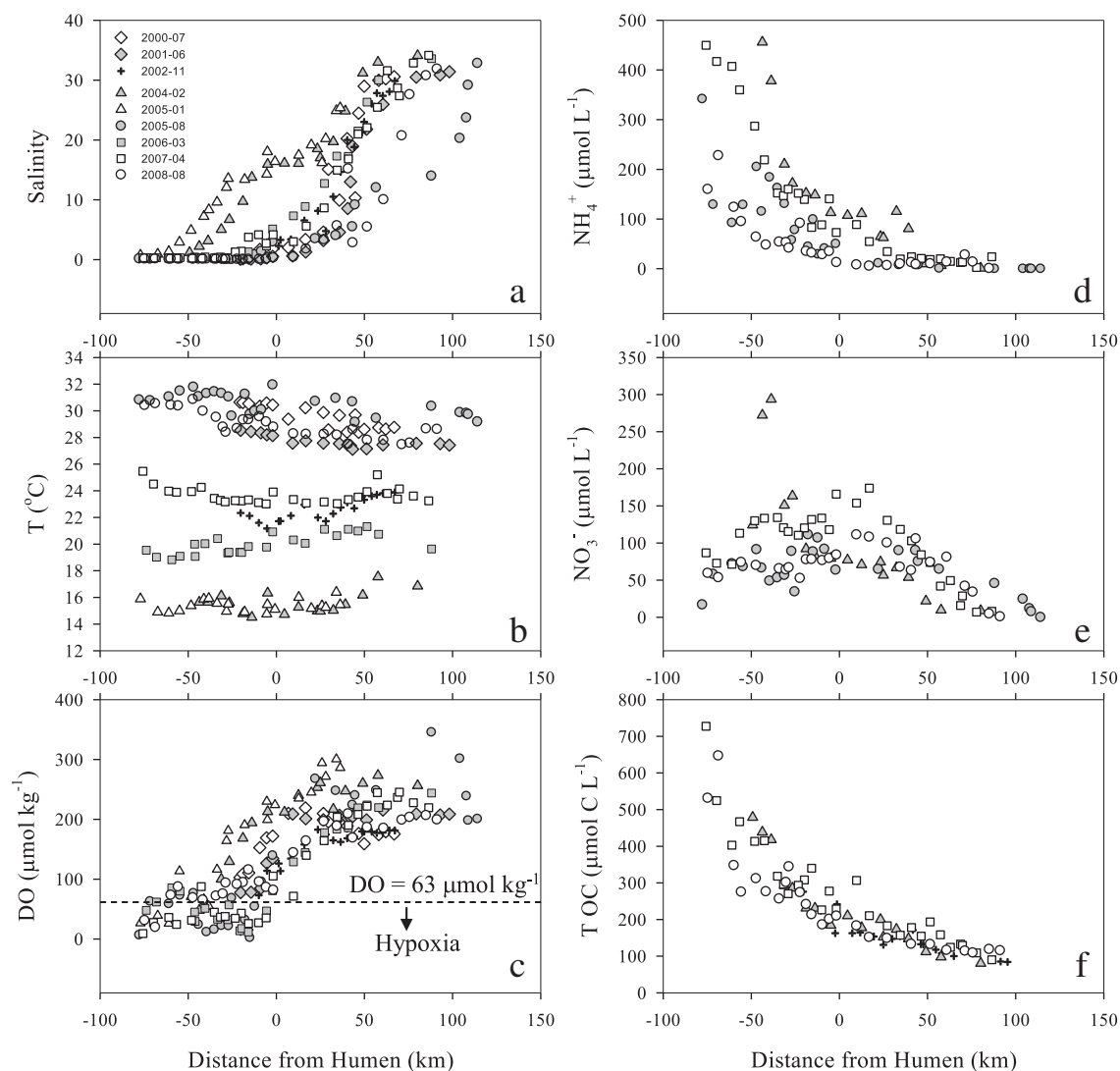
Fig. 2. The distribution of salinity (a), temperature (b), dissolved oxygen (c), NH_4^+ (d), NO_3^- (e), and total organic carbon (TOC, calculated as the sum of DOC and POC) (f) for the surface water of the Pearl River Estuary.

the Humen Outlet. In November 2002 (autumn) the observation area was relatively narrow, however from the limited data, the DO distribution was similar to spring. In winter, estuarine mixing played a significant role in raising the oxygen content upstream of Humen. Interestingly, there was a notable difference of surface DO distribution between the two summer seasons. Oxygen depletion was more serious in August 2005 than in August 2008 in the upper reaches, and the maximum oxygen concentration ($\sim$350 μmol O_2 kg^{-1}) was observed in the lower estuary in August 2005, but not in August 2008 (Fig. 2c).

3.3. Water column oxygen metabolism

3.3.1. Total oxygen consumption

Oxygen metabolism was measured at three stations in spring 2007 and eight stations in summer 2008 (Table 3). In the other cruises incubation was only carried out at Station 2. It should be pointed out that, because of the very low DO concentration in the upper reaches (e.g. the in situ DO was 2–9 μmol O_2 kg^{-1}) in spring 2007, the water had been bubbled with fresh air to enrich the oxygen before incubation. Through oxygen enriched incubation and in situ oxygen incubation, we found that the oxygen consumption rate could be enhanced 47% when the initial in situ oxygen was low (e.g. 31 μmol O_2 kg^{-1} at Station 1), but not changed significantly when the in situ oxygen was

higher than 91 μmol kg^{-1} (e.g. at Stations 3 and 4, Table 3). Given that the enrichment of oxygen could stimulate the oxygen consumption rates in the low initial DO situation, we referred to the oxygen consumption rate from the enriched incubation as the potential rate and that from in situ DO incubation as the in situ rate. Potential oxygen consumption rates could be considered as a measure of the aerobic biomass present at the time of sampling.

In situ total oxygen consumption rates showed strong spatial variability, with a range of 93–101 μmol O_2 L^{-1} d^{-1} at Station 1, and decreased sharply to 3.4 μmol O_2 L^{-1} d^{-1} at Station 8 in August 2008. A similar distribution pattern of potential total oxygen consumption rates was also observed in spring 2007. In terms of vertical distribution, in situ total oxygen consumption rates in surface water were similar to those in bottom water at Stations 1 and 2, whereas the total oxygen consumption rates in surface water were significantly higher than those in bottom water at Stations 3 and 5 (Table 3). These distribution patterns were similar to the profile of hydro-chemical parameters (data not shown).

3.3.2. Nitrification oxygen consumption

As shown in Table 3, the NH_4^+ oxidation rates ranged from 4.25 to 24.5 μmol N L^{-1} d^{-1} in April 2007 and from below the detection limit to 26.9 μmol N L^{-1} d^{-1} in August 2008 upstream of Humen. Similarly,

Table 3
Total oxygen consumption rates, nitrification rates and microbial respiration rates in the Pearl River Estuary during spring 2007 and summer 2008.

Cruises	Station	R_t	R_n		R_c	Initial DO (μmol O_2 kg^{-1})
			AOR	NOR		
April-2007	Sta.1	n.d.	12.6	3.07	n.a.	9
	Sta.2	125*	24.5	33.8	70.8*	31
	Sta.2$_b$	n.d.	20.4	33.6	n.a.	24
	Sta.3	61.9*	15.3	10.0	34.0*	38
	Sta.4	n.d.	8.78	13.9	n.a.	35
	Sta.5	19.2*	4.25	13.2	6.22*	105
August-2008	Sta.1	93.6 (138*)	26.9	15.4	45.6	31
	Sta.1$_b$	101	n.a.	n.a.	53.0	26
	Sta.2	65.0	12.0	2.64	45.7	69
	Sta.2$_b$	n.d.	13.1	3.53	n.a.	83
	Sta.3	60.2 (65.0*)	9.97	1.98	44.3	91
	Sta.3$_b$	21.4	n.a.	n.a.	5.42	88
	Sta.4	45.6 (39.1*)	17.5	n.d.	12.9	94
	Sta.5	21.1	n.d.	12.1	15.1	82
	Sta.5 (8 m)	13.9	n.a.	n.a.	7.87	70
	Sta.5$_b$	11.8	n.a.	n.a.	5.71	78
	Sta.6	11.5	n.d.	2.41	10.3	164
	Sta.7	7.19	n.d.	n.d.	7.19	189
	Sta.8	3.43	n.d.	n.d.	3.43	203

Note:

1) All samples were taken from the surface at ~1 m except at Station 5 in Aug. 2008. Stations with subscript b represent bottom water samples. Bottom waters were taken ~2 m above the sediment.
2) R_t represents the total oxygen consumption rate (μmol O_2 L^{-1} d^{-1}); R_n represents the nitrification rate (μmol N L^{-1} d^{-1}); R_c represents the microbial respiration rate (μmol O_2 L^{-1} d^{-1}), which is calculated as the difference by subtracting the nitrification oxygen consumption rate from the total oxygen consumption rate; data with an * are potential rates; AOR represents the ammonium oxidation rate; NOR represents the nitrite oxidation rate; n.a. represents no analysis; n.d. represents non detectable.

the NO_2^- oxidation rate ranged from 3.07 to 33.8 μmol N L^{-1} d^{-1} in April 2007 and from below the detection limit to 15.4 μmol N L^{-1} d^{-1} in August 2008. The downstream Humen nitrification rates were undetectable, which was probably due to NH_4^+ limitation and/or salinity inhibition.

3.3.3. Microbial respiration

Microbial respiration was high in the upper reaches of the estuary (Table 3). In summer, the highest respiration rate was measured in the Guangzhou Channel, with a range of 45.6–53.0 μmol O_2 L^{-1} d^{-1}, and then decreased to 5.7–15.1 μmol O_2 L^{-1} d^{-1} in the Humen Channel and to 3.4–10.3 μmol O_2 L^{-1} d^{-1} in Lingdingyang Bay (Table 3). A similar distribution pattern of respiration rates was observed in spring. Seasonally, the maximal values were observed in August 2005 with high water temperature and high total organic carbon (TOC) and NH_4^+ (Table 4).

3.3.4. Planktonic oxygen production

The median P_{max} estimated from surface Chl-a was also high in the Guangzhou Channel, with a range of 115–192 mmol C m^{-3} d^{-1} in April 2007 and 104–159 mmol C m^{-3} d^{-1} in August 2008, and decreased rapidly along the estuary to a value of 5.9 mmol C m^{-3} d^{-1} in the middle estuary in April 2007 and 4.6 mmol C m^{-3} d^{-1} in the lower estuary in August 2008 (Fig. 3c). This high P_{max} in the upper reaches of the estuary was probably due to the high phytoplankton biomass (i.e. 40 mg m^{-3} of Chl-a at Station 1 in spring 2007). However, the water column integrated rates of photosynthetic O_2 production (P_i) were much lower than the microbial respiration rates (Table 3 and Fig. 3d), which was due to the light limitation in the upper reaches. Our results suggested that the ecosystem was strongly heterotrophic in the upper reaches of the PRE. In the lower estuary the P_i was enhanced significantly in spring 2007 but not in summer 2008.

3.4. Air–water oxygen flux

The oxygen fluxes across the air–water interface were calculated based on Eqs. (5) and (6) and were shown in Fig. 3b. The upper reaches of the estuary had high O_2 influxes from the atmosphere year-round. In the mid-estuary (mixing-dominated zone) there was generally a sink of O_2 to the atmosphere in most parts of the year except in January 2005 and in August 2005. The air–water O_2 fluxes were −47 to 49 mmol O_2 m^{-2} d^{-1} (almost equilibrium) in January 2005, and −37 to −3.3 mmol O_2 m^{-2} d^{-1} (with an average of −21 ± 22 mmol O_2 m^{-2} d^{-1}) in August 2005, showing a weak source of atmospheric O_2.

In the lower estuary, the air–water O_2 fluxes indicated that there was still a weak sink for atmospheric O_2 in spring and autumn, but a weak source in winter. It was interesting to note that opposite results were observed in the two summer seasons. The lower estuary and inner shelf of SCS became a significant seasonal source of atmospheric O_2 due to the algal bloom in August 2005. In contrast, there was no phytoplankton bloom in the estuary in August 2008, due to the high river discharge (13,700 m^3 s^{-1} in August 2008 vs. 8600 m^3 s^{-1} in August 2005) pushing the estuarine plume out into the open coastal waters, and inducing a bloom in the outer SCS shelf (Dai et al., 2008b; Han et al., 2012; Yin et al., 2004).

4. Discussion

4.1. Factors influencing DO distribution

Factors contributing to the variations of DO in an estuarine system include freshwater discharge, estuarine circulation and mixing, as well as air–water O_2 exchange and biogeochemical processes.

4.1.1. River discharge and estuarine mixing

The Pearl River showed remarkable variations in freshwater discharge, with a range of ~2200 m^3 s^{-1} in the dry season (January 2005) and ~13,700 m^3 s^{-1} (the sum of three tributaries) in the wet season (August 2008) during our observation cruises. This high variation of river discharge had a significant impact on estuarine water mixing and the distribution of organic carbon and nutrients, and therefore influenced the DO distribution. As shown in Fig. 4, the average DO% in the Humen Channel and Shiziyang Channel (considering the data available) was positively correlated with the monthly average discharge of the Humen Outlet except in the very low flow winter seasons. This was probably due to high river discharge that diluted the nutrients and organic mater, and consequently reduced the oxygen consumption rate. On the other hand, high river discharge could effectively shorten the flushing time of the water and facilitate aeration; whereas in the dry season, seawater occupied the whole estuary, and the salt wedge could intrude up to 50–70 km upstream of Humen (Fig. 2a). Mixing with high DO seawater likely played a significant role in raising the oxygen content upstream of Humen in dry seasons. As such, DO showed a significant (P < 0.01) and positive correlation with salinity (Table 5) only in winter (e.g. February 2004), indicating again that estuarine mixing was another important factor controlling the distribution of DO in this season.

4.1.2. Biogeochemical processes

Processes that may drawdown DO concentration include microbial respiration and nitrification. The sources of DO include photosynthesis and supply from air–water exchange.

In the upper reaches of the estuary, light penetration is expected to be low due to the absorption and scatterance of light by high DOC and TSM. Therefore, the contribution of photosynthesis to the DO should be low due to the light limitation. In contrast, high values of 20–40 mg m^{-3} in Chl-a were observed in the Guangzhou Channel in spring and summer. In such cases, phytoplankton stock may be the feed of the accumulation of Chl-a biomass due to the longer flushing time in this particular section

Table 4
Biogeochemical parameters and total oxygen consumption rates at Station 2 during different cruises.

Cruises	DO	TOC	NH_4^+	Temperature	R_t	$^S R_t$	$^{20}R_t$
	(μmol O_2 kg^{-1})	(μmol C L^{-1})	(μmol L^{-1})	(°C)			
February-2004	48	796	456	15.64	115	318	229
August-2005	24	496	115	31.08	164	2870	29
March-2006	29	412	378	19.21	56	361	63
April-2007	31	413	287	23.95	125	1050	67
August-2008	69	312	64	30.87	65	3254	12

R_t represents total oxygen consumption rate (μmol O_2 L^{-1} d^{-1}); $^S R_t$ represents TOC and NH_4^+ normalized total oxygen consumption rate (in units of μmol O_2 L^{-1} d^{-1} (mmol C L^{-1})$^{-1}$ (mmol N L^{-1})$^{-1}$). $^S R_t$ was calculated with site measurement oxygen consumption rates divided by site initial TOC and NH_4^+ concentrations, which was used to denote per mmol L^{-1} TOC and per mmol L^{-1} NH_4^+ oxygen consumption rate; $^{20}R_t$ represents temperature normalized (T = 20 °C) total oxygen consumption rate (μmol O_2 L^{-1} d^{-1}). $^{20}R_t$ was calculated using the regression kinetics equation ($^{20}R_t = R_t \times e^{0.1579(20 - T)}$), where T is the in situ temperature.

of the river channel. High Chl-a concentration may also be reflective of the inputs from upstream as observed in the Hudson River estuary (Cole et al., 1992), and/or the absence of grazers in this hypoxic zone as reported in the upper reaches of the Scheldt Estuary (Kromkamp et al., 1995).

Microorganisms are the key players in consuming DO through respiration (oxidation of organic matter) and nitrification (oxidation of NH_4^+). Aerobic bacteria convert organic matter to CO_2, consuming 1 mol of oxygen per mole of organic carbon. Oxidation of NH_4^+ to nitrate requires 2 mol of oxygen per mole of NH_4^+.

As shown in Fig. 2, the individual chemical species varied strongly along the estuary. The lowest DO in surface water observed in the Guangzhou Channel corresponded to the highest concentrations of NH_4^+ and TOC. Downstream in the Guangzhou Channel, NH_4^+ and TOC decreased sharply whereas NO_3^- increased rapidly, indicating that nitrification and organic matter oxidation should be the main processes controlling the oxygen depletion in the upper reaches of the estuary.

DO was significantly (P < 0.05 or P < 0.01) and negatively correlated with NH_4^+, DOC and POC concentrations (Table 5) in both summer and

winter. This again suggested that the high loads of NH_4^+ and organic matter (DOC and POC) fueled the heavy microbial respiration and nitrification upstream of Humen. In contrast, DO was not significantly correlated with NH_4^+, DOC and POC concentrations in spring 2007. This was probably due to the very high concentrations of DOC, POC and NH_4^+ (Fig. 2) which were far beyond the threshold that the organisms could consume. This was also inferred by the very low DO saturation (<30%, Fig. 3a) throughout the whole section (~75 km) from Humen to the suburbs of Guangzhou. A poor correlation between nitrifying activity and inorganic nitrogen was also found in a previous study in this area (Dai et al., 2008a).

4.1.3. Temperature

Under fixed salinity and pressure, DO saturation concentration is a function of temperature. The relatively higher DO in winter was partially due to the enhancement of the DO solubility at low temperature. However, it should be noted that DO concentration in the upper reaches of the PRE was far below the saturation concentration. Temperature may also affect the gas exchange in two ways. First, temperature can
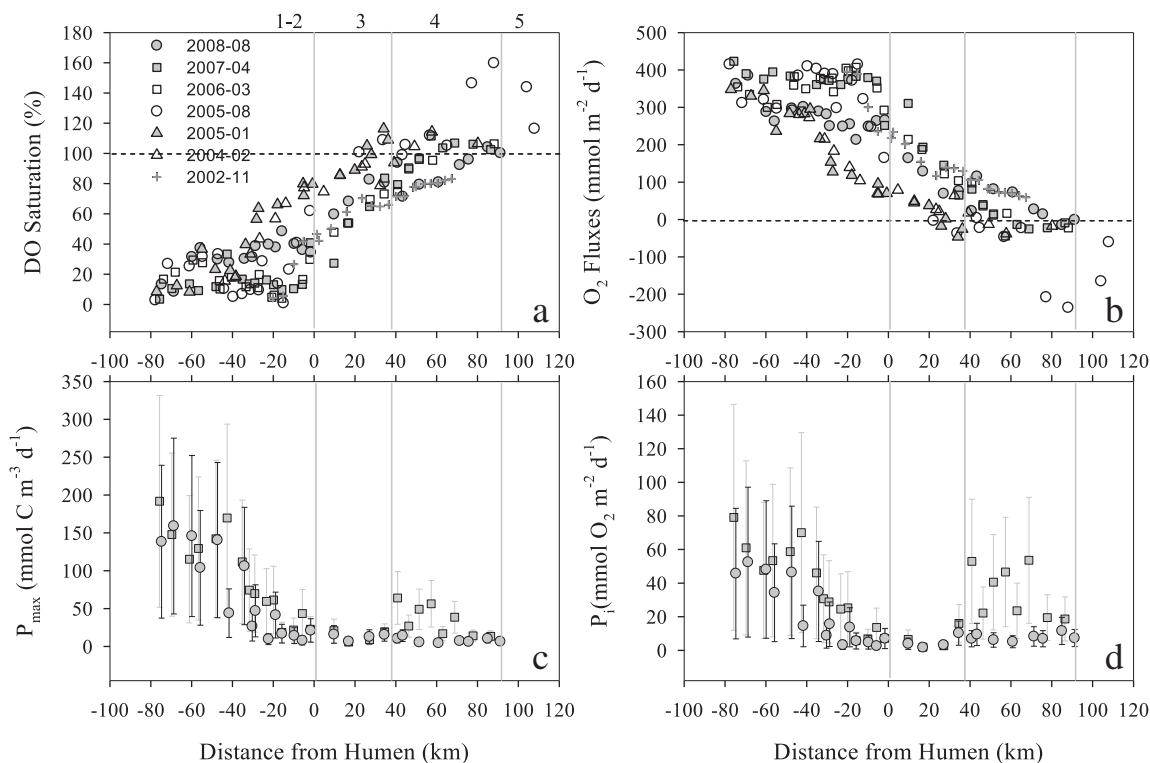

Fig. 3. Spatial distribution of dissolved oxygen saturation (a), air–water O_2 exchange fluxes (b), optimal primary production (P_{max}) estimated from Chl-a (c), and water column integrated primary production (P_i) (d) in the PRE. The distance is positive for downstream and negative for upstream of Humen. Horizontal lines in panel a represent 100% dissolved oxygen saturation, and in panel b they represent 0 O_2 flux. Vertical lines represent the boundaries of the different parts of the Pearl River Estuary: 1–2, upper reaches; 3, mid-estuary; 4, lower estuary; 5, inner shelf.
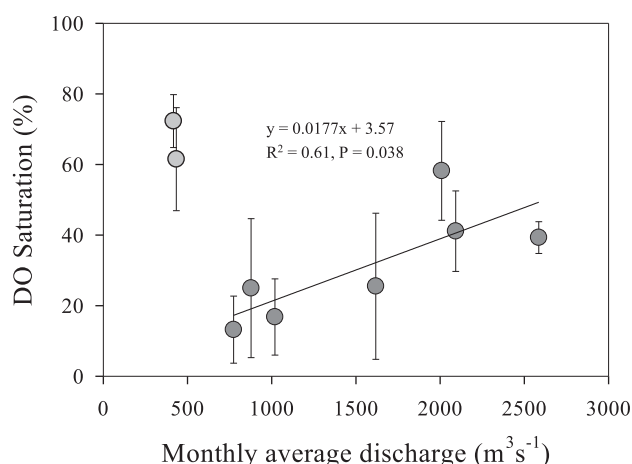
Fig. 4. Average surface dissolved oxygen saturation (DO%) from Humen to Shiziyang versus monthly average discharge of the Humen Outlet. The line represents the regression curve (excluding February 2004 and January 2005).

affect the diffusivity. Second, temperature also affects momentum transport across the air–sea interface because both the density of air and the kinematic viscosity of water are temperature dependent. According to the equation presented by Hartman and Hammond (1985), the liquid phase gas transfer coefficient will increase 2.3–3.1% (for fresh water) and 2.1–2.7% (for sea water) when the temperature increases by 1 °C. This section will focus on the effect of temperature on the biogeochemical processes.

Total oxygen consumption rates measured onboard at Station 2 (~45 km upstream of the Humen Outlet) showed no obvious correlation with temperature (Table 4). This was probably due to the co-variation of other factors (e.g. NH_4^+ and TOC concentrations) with water temperature. Poor correlation between respiration and temperature is also found in the Urdaibai Estuary, Spain, which receives substantial inputs of organic matter from a sewage treatment plant (Iriarte et al., 1997). When we normalized total oxygen consumption rate with TOC and NH_4^+ concentration to per milli-mole (^SR_t in Table 4), ^SR_t had a significant, exponential correlation with temperature. The regression equation was $^SR_t = 22.60 \times e^{0.1579T}$ ($R^2 = 0.98$). The R^2 of the regression indicated that temperature explained 98% of the variation of substrate (TOC and NH_4^+) normalized total oxygen consumption rates. From the regression equation, the calculated apparent Q_{10} value was 4.85 in the upper reaches of the estuary (Q_{10} represents the increase in the rate of a process at each 10 °C increase in temperature). This value was in line with the typical range of 2–4 for the enzyme-catalyzed reaction, but significantly higher than the Q_{10} estimated for nitrification in the same area (Dai et al., 2008a). This discrepancy may be partially due to the fact that the total oxygen consumption was not only associated with bacterial and phytoplankton respiration but also with nitrification, which has different values of Q_{10} (Berounsky and Nixon, 1990). It is also because the method for Q_{10} estimation in the present study is different

from that in Dai et al. (2008a). In the present study, the Q_{10} was estimated from the relationship between ^SR_t and temperature. The substrate normalized rates excluded the influence of concentration that might better reflect the influence of the temperature because the concentrations of NH_4^+ and TOC were much higher in winter than in summer.

On the other hand, we normalized the total oxygen consumption rate to a temperature of 20 °C ($^{20}R_t$, Table 4), and examined the simultaneous effects of TOC and NH_4^+ on $^{20}R_t$ using multiple linear regression (software SPSS 11.0). The regression equation was $^{20}R_t = (0.322 \pm 0.107) \times TOC + (0.188 \pm 0.118) \times C_N - (125.3 \pm 41.3)$ ($R^2 = 0.941$). The R^2 of the regression between $^{20}R_t$ and TOC and NH_4^+ concentrations indicated that TOC and NH_4^+ inputs could explain 94% of the variation in temperature normalized total oxygen consumption rates. Both results suggested that substrate supply and temperature were two major factors controlling the magnitude of total oxygen consumptions in the water column.

From the regression equation, we found that a 1 µmol L^{-1} decrease in TOC input could reduce 0.322 µmol O_2 L^{-1} d^{-1} of oxygen consumption rate, while a 1 µmol L^{-1} decrease in NH_4^+ input could reduce 0.188 µmol O_2 L^{-1} d^{-1} of oxygen consumption rate, implying that organic matter respiration contributed in the same magnitude but in a higher portion to the total oxygen consumption than nitrification. This finding was further supported by the microbial respiration oxygen consumption rates and nitrification oxygen consumption rates of the incubation stations (Table 3).

4.2. Mass balance of DO upstream of Humen

Here, we applied a simple box model to see if the DO could be mass-balanced in the oxygen depletion area upstream of the Humen Outlet. We confined the model to summer when our field data were most complete. In the summer cruises, the salinity was ~0 upstream of the Humen Outlet and the water column was almost well mixed.

For the oxygen mass-balance model, factors including sediment O_2 consumption, nitrification and aerobic respiration oxygen consumption in the water column, photosynthesis, advective transport, and water–air exchange were considered. Considering that the oxygen depleted zone extended from Humen to the suburbs of Guangzhou, covering ~75 km of water body, and that the gradient of DO was small (<1 µmol km^{-1}), the dispersion flux in our model calculation was ignored. Assuming that the system is in steady state, the mass-balance formula can be expressed as follows:

$$F_{a-w} \times A + P_i \times A + R_s \times A + R_c \times A \times H + R_n \times A \times H + F_{h-in} + F_{h-out} = 0 \quad (9)$$

where F_{a-w} is the section average air–water exchange flux (mmol m^{-2} d^{-1}); P_i is the integrated gross photosynthetic production flux (mmol m^{-2} d^{-1}); R_s is the sediment oxygen consumption flux (mmol m^{-2} d^{-1}); R_c and R_n are the microbial respiration rate and nitrification rate (mmol m^{-3} d^{-1}); and F_{h-in} and F_{h-out} are DO input and

Table 5

The correlation coefficient between surface water dissolved oxygen (DO), ammonium (NH_4^+), dissolved organic carbon (DOC), particulate organic carbon (POC), and salinity (S) in the upstream of Humen outlet, the Pearl River Estuary.

Parameter	February 2004 (n = 7)					April 2007 (n = 15)					August 2008 (n = 15)				
	DO	NH_4^+	DOC	POC	S	DO	NH_4^+	DOC	POC	S	DO	NH_4^+	DOC	POC	S
DO	1	−0.912[a]	−0.964[a]	−0.766[b]	0.977[a]	1	−0.412	−0.356	−0.441	0.249	1	−0.811[a]	−0.896[a]	−0.811[a]	−0.314
NH_4^+		1	0.977[a]	0.914[a]	−0.827[b]		1	0.938[a]	0.612[b]	−0.669[a]		1	0.899[a]	0.867[a]	0.115
DOC			1	0.835[b]	−0.905[a]			1	0.704[a]	−0.519[b]			1	0.860[a]	0.223
POC				1	−0.673				1	−0.473				1	0.104
S					1					1					1

The most upper section was not survey in November 2002.

[a] Shows the statistical significance at P < 0.01.

[b] Shows the statistical significance at 0.01 ≤ P < 0.05.

Table 6
Dissolved oxygen (DO, μmol kg^{-1}) mass balance showing contributions from microbial and physical processes in the upper reaches of the Pearl River Estuary.

Sections	Input			Output			R_c	R_n	R_s	P_i	F_{a-w}	Area $\times 10^6$ (m^2)	Depth (m)
	Q_{in}	DO	F_{h-in}	Q_{out}	DO	F_{h-out}	mmol O$_2$ m^{-3} d^{-1}		mmol O$_2$ m^{-2} d^{-1}				
Section-1	286[a]	29	0.72	286	76	−1.9	−47.5	−34.2	−11.9	48.6	319	16.3	5.0
Section-2	520[b]	76	3.41	9853[e]	79	−67.3	−25.4	−17.1	−28.8	15.3	265	103.4	6.6
	2168[c]	102	19.1										
	7165[d]	78	48.3										

Q_{in} and Q_{out} represent water discharge in and out of the Sections (in units of m^3 s^{-1}) (China MWR-BH (Bureau of Hydrology, Ministry of Water Resources, China), 2009); superscript a represents the water discharge to Section 1 from the Guangzhou Channel; b represents the water discharge to Section 2 from Huangpu (including output from Section 1); c represents the water discharge to Section 2 from the East River; d shows the tidal influx volume to Section 2 from Humen (Zhao, 1990). e represents total water flux out of the Humen Outlet. F_{h-in} and F_{h-out} are the oxygen input and output fluxes by horizontal advection (10^6 mol d^{-1}). R_c, R_n, R_s, P_i and F_{a-w} represent the sectional average rates of microbial respiration, nitrification, sediment oxygen consumption, integrated photosynthetic O$_2$ production and air–water oxygen flux, respectively.

output by horizontal advection (mol d^{-1}). A is the section area (m^2); H is the section average depth of the water column (m).

Considering the strongly spatial variation of biological processes and topography, the upper reaches of the PRE can be divided into two sections: Section 1 ranged from Station 1 to Station 2 (i.e. the Guangzhou Channel) and Section 2 from Station 2 to Station 5 (i.e. the Huangpu, Shiziyang and Humen Channels). For the calculation of the section average biological oxygen consumption rates, an identical nitrification rate in the water column was assumed. It is reported that the nitrification rate in the water column is almost the same in this study area (Dai et al., 2008a). In the Guangzhou Channel (Station 1 to Station 2), microbial respiration rates in the surface water were similar to those in the bottom water, but, in the Shiziyang Channel and the Humen Channel (Station 3 to Station 5), the rates in the surface water were considerably higher than those in the bottom water (Table 3). So, for the model, the respiration rate of one site was chosen as the average respiration rate of the water column. Thus, the calculated average respiration rate and nitrification rate for Section 1 were 47.5 ± 2.5 mmol O$_2$ m^{-3} d^{-1} and 34.2 ± 19.5 mmol O$_2$ m^{-3} d^{-1}, while the average microbial respiration rate and nitrification rate for Section 2 were 25.5 ± 15.0 mmol O$_2$ m^{-3} d^{-1} and 17.1 ± 8.4 mmol O$_2$ m^{-3} d^{-1}.

The potential sediment oxygen consumption rates reported in the Guangzhou Channel are 11.9–28.8 mmol O$_2$ m^{-2} d^{-1} (Liu and Qi, 1994). Here we adopted 11.9 mmol O$_2$ m^{-2} d^{-1} and 28.8 mmol O$_2$ m^{-2} d^{-1} as the sediment oxygen consumption rates in Sections 1 and 2 for the model calculation. These values might represent the upper limit of the sediment oxygen consumption, because the low DO concentration in the water column upstream of Humen may inhibit sediment oxygen consumption (Kemp et al., 1992).

Air–water flux (Fig. 3b) was calculated using Eqs. (5) and (6), and the arithmetic average values within the sections were used in the model calculation. Advective oxygen flux was calculated as the multiplication between the boundary DO concentration and water discharge. The biological process fluxes and relevant parameters are listed in Table 6.

The results of these model calculations are presented in Fig. 5. The total oxygen input (105.0×10^6 mol O$_2$ d^{-1}) was nearly balanced by the total output (-106.1×10^6 mol O$_2$ d^{-1}), indicating that the system was not far from a steady state. The advective fluxes of DO (69.6×10^6 mol O$_2$ d^{-1} input, -67.3×10^6 mol O$_2$ d^{-1} output) were remarkable, but their net contribution to the oxygen budget was quite small (2.3×10^6 mol O$_2$ d^{-1}). The microbial respiration and nitrification in the water column were the main processes which controlled oxygen depletion in the upper reaches of the PRE. The oxygen consumption fluxes by respiration and by nitrification were -21.3×10^6 mol O$_2$ d^{-1} (accounting for 59% of the total oxygen consumption in the water column) and -14.5×10^6 mol O$_2$ d^{-1} (accounting for 41% of the total oxygen consumption in the water column). Reaeration (32.6×10^6 mol d^{-1}) was the key process controlling the oxygen complement. Contributions from other processes, such as phytoplankton photosynthesis (2.8×10^6 mol O$_2$ d^{-1}) and sediment oxygen consumption (3.2×10^6 mol O$_2$ d^{-1}), were secondary and minor.

Based on our simplified model, it was suggested that organic matter and ammonia stimulated the intense heterotrophic respiration and nitrification in the water column, which were sufficient to overwhelm oxygen production by autotrophs and supply from the reaeration result in drawing DO down to a low concentration. When the DO concentrations decreased continually, the air–water O$_2$ gradients would gradually increase, thereby increasing physical transport to the site. When the oxygen consumption was balanced by oxygen regeneration, the very low DO concentrations were maintained. Such a coupling of physical and biological processes in the water column implied that any decrease in biological O$_2$ consumption would result in reduction in air–water O$_2$ gradient which would decrease O$_2$ replenishment through air–water exchange. Thus, it could be expected that any reduction in organic carbon and ammonia loading to the PRE would result in rapid but proportionally smaller increases in dissolved O$_2$ concentrations.
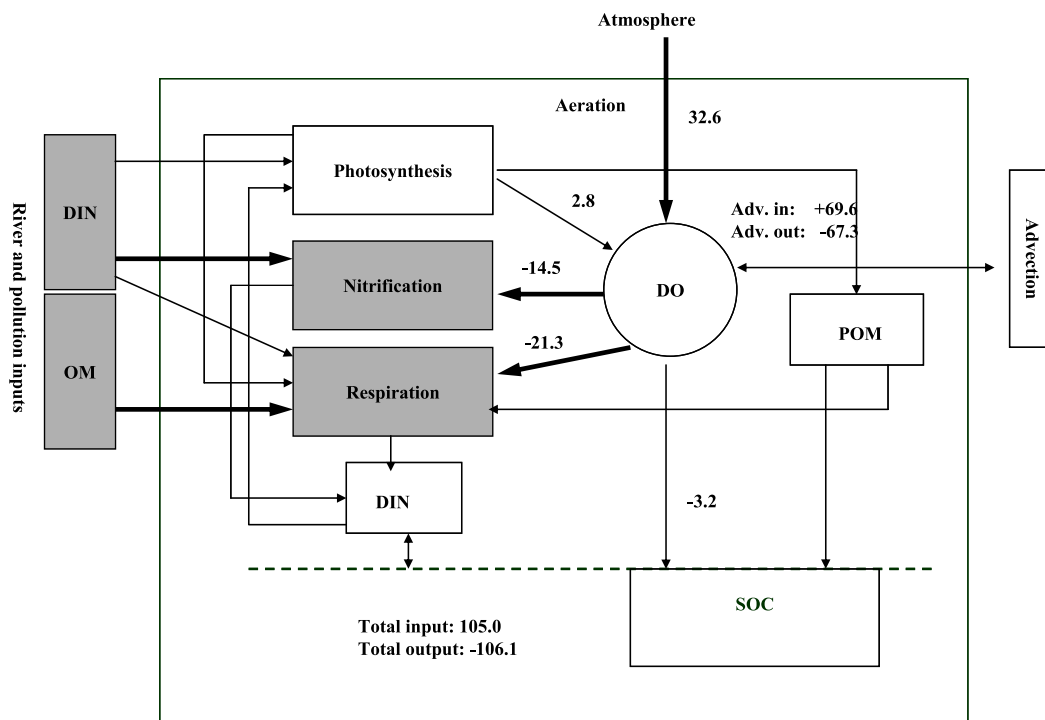
Fig. 5. Conceptual model showing the formation of hypoxia at the upstream of Humen. Sediment oxygen consumption (SOC) rates are after Liu and Qi (1994). The unit of the fluxes is 10^6 mol O_2 d^{-1}.

Downstream of the Humen Outlet, microbial respiration rates were rapidly decreased seaward and the nitrification rates were almost below the detection limit. So the air–water fluxes were significantly higher than the biological oxygen consumption fluxes. As a result, the DO concentration was continually increasing seawards. At Station 8 in the lower estuary the surface DO was almost saturated.

4.3. The uncertainty of the DO budget

The results of the model simulation showed that the air–water fluxes were the most important processes impacting on the DO budget. These fluxes were calculated on the basis of O_2 concentrations and gas transfer velocity. The spatial variation of DO concentrations might introduce ~10% variability of this flux estimation. Based on the Wanninkhof (1992) empirical function, wind speed is the most important factor influencing the air–water flux. Another uncertainty of the DO budget was introduced by the largely spatial variability of respiration rates (e.g. 47.5 ± 2.5 μmol O_2 L^{-1} in Section 1, and 25.5 ± 15.0 μmol O_2 L^{-1} d^{-1} in Section 2) and nitrification rates (e.g. 34.2 ± 19.5 μmol O_2 L^{-1} d^{-1} in Section 1, and 17.1 ± 8.4 μmol O_2 L^{-1} d^{-1} in Section 2). These spatial variations will introduce at most ~33% uncertainty in the calculation of the total oxygen consumption (i.e. by respiration and nitrification) in the water column, or ~30% uncertainty in the budget of the total oxygen consumption. There might also be uncertainties in the adoption of sediment oxygen consumption rates and in the estimation of the photosynthetic rates. However, the contributions of these two processes to the DO budget were rather small in the upper reaches of the estuary. For example, doubling the assumed sediment oxygen consumption rates, from 11.9 to 23.8 mmol O_2 m^{-2} d^{-1} for Section 1 and from 28.8 to 57.6 mmol O_2 m^{-2} d^{-1} for Section 2, would increase the calculated oxygen consumption flux by only ~8%. The uncertainty of photosynthetic rate estimation was at most 85% (see discussion in Section 2.4). Increasing or reducing photosynthetic production by 85% would introduce <7% of change in the calculated oxygen supply flux.

4.4. The origin of the organic matter supporting microbial respiration

To calculate the organic carbon budget, the mass balance model formula used was as follows:

$$\frac{\partial C}{\partial t} = F_{in} + F_{out} + F_a + F_P + F_b + F_R \tag{10}$$

where C is the concentration of TOC, F_{in} and F_{out} are the river input and the net downstream transport, F_a is atmospheric deposition, F_P is primary production, F_b is sedimentary burial flux, and F_R is the TOC consumption flux by microbial respiration. Assuming that the system is in a steady state, then $\frac{\partial C}{\partial t} = 0$, and so we obtain:

$$F_{in} + F_{out} + F_a + F_P + F_b + F_R = 0. \tag{11}$$

The river input and the net downstream export of TOC were calculated as the boundary TOC concentration multiplied by water discharge, which is similar to the calculation of advective oxygen flux. The river input of TOC was estimated as $+74.1 \times 10^6$ mol C d^{-1}, and the net downstream output as -57.4×10^6 mol C d^{-1}. The atmospheric deposition of TOC was not available, but the average deposition of organic nitrogen in the PRE was around 3.88 kg N km^{-2} d^{-1} (Chen et al., 2010). Given that the mean C/N mole ratio of terrestrial organic matter is 12 (Hedges and Oades, 1997), this deposition was equivalent to 39.9 kg C km^{-2} d^{-1}. Thus, the atmospheric deposition of TOC in the studied area was $+3.98 \times 10^5$ mol C d^{-1}. The primary production estimated from Chl-a was $+2.24 \times 10^6$ mol C d^{-1} (or $+2.78 \times 10^6$ mol O_2 d^{-1}). Based on the sedimentary rate (0.59 ± 0.40 g cm^{-1} yr^{-1}) and organic carbon content ($1.2\% \pm 0.45\%$) of the sediment reported in this area (He et al., 2010a; Lin et al., 1998), the average sedimentary burial was -1.96×10^6 mol C d^{-1}. Thus the loss of TOC by microbial respiration was estimated as -17.4×10^6 mol C d^{-1}. The in situ primary production only supported $13\% \pm 10\%$ of organic carbon consumption in this oxygen depletion area.

5. Conclusions

We confirmed that serious oxygen depletion occurred year-round throughout the water column in the upper reaches of the PRE. Our simplified model demonstrated an example of the formation and maintenance mechanism of hypoxia in the highly polluted, turbid, and well mixed estuary. The oxygen depletion happened primarily in the water column rather than in the benthic. Microbial respiration and nitrification were the major processes controlling the oxygen consumption, and accounted for respectively 59% and 41% of the total oxygen consumption in the water column. This study confirmed the importance of the allochthonous organic matter and ammonia in forming and maintaining the oxygen depletion in the estuary. Thus, controlling both sewage discharge and local urban runoff is more important than reducing the nutrient loading from upstream nonpoint sources in order to improve water quality in this particular environmental setting, which is probably also true of some other estuarine and coastal systems with high turbidity.

References

Benson, B.B., Krause, D., 1984. The concentration and isotopic fractionation of oxygen dissolved in fresh water and seawater in equilibrium with the atmosphere. Limnol. Oceanogr. 29, 620–632.

Berounsky, V.M., Nixon, S.W., 1990. Temperature and the annual cycle of nitrification in waters of Narragansett Bay. Limnol. Oceanogr. 35 (7), 1610–1617.

Cai, Y., Ning, X., Liu, Z., 2002. Studies on primary production and new production of the Zhujiang Estuary, China. Acta Oceanol. Sin. 24 (3), 101–111 (in Chinese).

Chen, Z., Li, K., Lin, W., Liu, A., 2010. Atmospheric dry and wet deposition of nitrogen and phosphorus in the Pearl River Estuary. Environ. Pollut. Control 32 (11), 53–57 (in Chinese).

China MWR-BH (Bureau of Hydrology, Ministry of Water Resources, China), 2009. China Hydrological Information Annual Report 2008. China Water Power Press, Beijing, China (128 pp., in Chinese).

Cole, J.J., Caraco, N.F., Peierls, B.L., 1992. Can phytoplankton maintain a positive carbon balance in a turbid, freshwater, tidal estuary? Limnol. Oceanogr. 37 (8), 1608–1617.

Dai, M., Guo, X., Zhai, W., Yuan, L., Wang, B., Wang, L., Cai, P., Tang, T., Cai, W.-J., 2006. Oxygen depletion in the upper reach of the Pearl River Estuary during a winter drought. Mar. Chem. 102 (1–2), 159–169.

Dai, M., Wang, L., Guo, X., Zhai, W., Li, Q., He, B., Kao, S.-J., 2008a. Nitrification and inorganic nitrogen distribution in a large perturbed river/estuarine system: the Pearl River Estuary, China. Biogeosciences 5, 1227–1244.

Dai, M., Zhai, W., Cai, W., Callahan, J., Huang, B., Shang, S., Huang, T., Li, X., Lu, Z., Chen, W., Chen, Z., 2008b. Effects of an estuarine plume-associated bloom on the carbonate system in the lower reaches of the Pearl River estuary and the coastal zone of the northern South China Sea. Cont. Shelf Res. 28 (12), 1416–1423.

Dai, M., Lu, Z., Zhai, W., Chen, B., Cao, Z., Zhou, K., Cai, W., Chen, C., 2009. Diurnal variations of surface seawater $p\mathrm{CO_2}$ in contrasting coastal environments. Limnol. Oceanogr. 54 (3), 735–745.

Dai, M., Gan, J., Han, A., Kung, H.S., Ying, Z., 2014. Physical dynamics and biogeochemistry of the Pearl River plume. In: Bianchi, T.S., Allison, M.A., Cai, W. (Eds.), Biogeochemical Dynamics at Large River–Coastal Interfaces. Cambridge University Press, Cambridge, pp. 321–352 (Chapter 13).

Diaz, R.J., Rosenberg, R., 2008. Spreading dead zones and consequences for marine ecosystems. Science 321 (5891), 926–929.

Frankignoulle, M., Bourge, I., Wollast, R., 1996. Atmospheric $\mathrm{CO_2}$ fluxes in a highly polluted estuary (the Scheldt). Limnol. Oceanogr. 41 (2), 365–369.

Garnier, J.P., Servais, G., Billen, M.A., Brion, N., 2001. Lower Seine River and estuary (France) carbon and oxygen budget during low flow. Estuaries 24 (6), 964–976.

Guo, X., Dai, M., Zhai, W., Cai, W., Chen, B., 2009. $\mathrm{CO_2}$ flux and seasonal variability in a large subtropical estuarine system, the Pearl River Estuary, China. J. Geophys. Res. Biogeosci. 114, G03013. http://dx.doi.org/10.1029/2008JG000905.

Hagy, J.D., Boynton, W.R., Keefe, C.W., Wood, K.V., 2004. Hypoxia in Chesapeake Bay, 1950–2001: long-term change in relation to nutrient loading and river flow. Estuaries 27 (4), 634–658.

Han, A., Dai, M., Kao, S.-K., Gan, J., Li, Q., Wang, L., Zhai, W., Wang, L., 2012. Nutrient dynamics and biological consumption in a large continental shelf system under the influence of both a river plume and coastal upwelling. Limnol. Oceanogr. 57 (2), 486–502.

Hartman, B., Hammond, D.E., 1985. Gas exchange in San Francisco Bay. Hydrobiologia 129 (1), 59–68.

He, B., Dai, M., Huang, W., Liu, Q., Chen, H., Xu, L., 2010a. Sources and accumulation of organic carbon in the Pearl River Estuary surface sediment as indicated by elemental, stable carbon isotopic, and carbohydrate compositions. Biogeosciences 7, 3343–3362.

He, B., Dai, M., Zhai, W., Wang, L., Wang, K., Chen, J., Lin, J., Han, A., Xu, Y., 2010b. Distribution, degradation and dynamics of dissolved organic carbon and its major compound classes in the Pearl River estuary, China. Mar. Chem. 119 (1–4), 52–64.

Hedges, J.I., Oades, J.M., 1997. Comparative organic geochemistries of soils and marine sediments. Org. Geochem. 27 (7–8), 319–361.

Huang, B., Hong, H., Ke, L., Cao, Z., 2005. Size-fractioned phytoplankton biomass and productivity in the Zhujiang River Estuary in China. Acta Oceanol. Sin. 27 (6), 180–187 (in Chinese).

Iriarte, A., de Madariaga, I., Diez-Garagarza, F., Revilla, M., Orive, E., 1997. Primary plankton production, respiration and nitrification in a shallow temperate estuary during summer. J. Exp. Mar. Biol. Ecol. 208 (1), 127–151.

Justic, D., Rabalais, N.N., Turner, R.E., 2002. Modeling the impacts of decadal changes in riverine nutrient fluxes on coastal eutrophication near the Mississippi River Delta. Ecol. Model. 152 (1), 33–46.

Kemp, W.M., Sampou, P.A., Garber, J., Tuttle, J., Boynton, W.R., 1992. Seasonal depletion of oxygen from bottom waters of Chesapeake Bay: roles of benthic and planktonic respiration and physical exchange processes. Mar. Ecol. Prog. Ser. 85 (1), 137–152.

Kromkamp, J., Peene, J., van Rijswijk, P., Sandee, A., Goosen, N., 1995. Nutrients, light and primary production in the eutrophic, turbid Westerscheldt estuary (The Netherlands). Hydrobiologia 311 (1–3), 9–19.

Lee, Y.J., Lwiza, K.M.M., 2008. Characteristics of bottom dissolved oxygen in Long Island Sound, New York. Estuar. Coast. Shelf Sci. 76 (2), 187–200.

Lin, R., Min, Y., Wei, K., Zhang, G., Yu, F., Yu, Y., 1998. ^{210}Pb-data of sediment cores from the Pearl River mouth and its environmental geochemistry implication. Geochimica 27 (5), 401–411 (in Chinese).

Lin, J., Xu, H., Cudaback, C., Wang, D., 2008. Inter-annual variability of hypoxic conditions in a shallow estuary. J. Mar. Syst. 73 (1–2), 169–184.

Liu, F., Qi, S., 1994. Sediment oxygen demand in the Yuancun reach of the Pearl River in Guangzhou. Chin. J. Environ. Sci. 15 (1), 31–35 (in Chinese).

Oviatt, C., Rudnick, D., Leller, A., Sampou, P., Almquist, G., 1986. A comparision of system ($\mathrm{O_2}$ and $\mathrm{CO_2}$) and C-14 measurements of metabolism in estuarine mesocosms. Mar. Ecol. Prog. Ser. 28, 57–67.

Parsons, T.R., Maita, Y., Lalli, C.M., 1984. A Manual of Chemical and Biological Methods for Seawater Analysis. Pergamon Press, Oxford (173 pp.).

Platt, T., Sathyendranath, S., 1993. Estimators of primary production for interpretation of remotely sensed data on ocean color. J. Geophys. Res. 98 (C8), 14561–14576.

Rabouille, C., Conley, D.J., Dai, M.H., Cai, W.J., Chen, C.T.A., Lansard, B., Green, R., Yin, K., Harrison, P.J., Dagg, M., McKee, B., 2008. Comparison of hypoxia among four river-dominated ocean margins: the Changjiang (Yangze), Mississippi, Pearl and Rhone rivers. Cont. Shelf Res. 28 (12), 1527–1537.

Ryther, J.H., 1956. The measurement of primary production. Limnol. Oceanogr. 1 (2), 72–84.

Ryther, J.H., Yentsch, C.S., 1957. The estimation of phytoplankton production in the ocean from chlorophyll and light data. Limnol. Oceanogr. 2 (3), 281–286.

Scavia, D., Rabalais, N.N., Turner, R.E., Justic, D., 2003. Predicting the response of Gulf of Mexico hypoxia to variations in Mississippi River nitrogen load. Limnol. Oceanogr. 48 (3), 951–956.

Skjelvan, I., Falck, E., Anderson, L.G., Rey, F., 2001. Oxygen fluxes in the Norwegian Atlantic current. Mar. Chem. 73 (3–4), 291–303.

Turner, R.E., Rabalais, N.N., Swenson, E.M., Kasprzak, M., Romaire, T., 2005. Summer hypoxia in the northern Gulf of Mexico and its prediction from 1978 to 1995. Mar. Environ. Res. 59 (1), 65–77.

Verity, P.G., Alber, M., Bricker, S.B., 2006. Development of hypoxia in well-mixed subtropical estuaries in the southeastern USA. Estuar. Coasts 29 (4), 665–673.

Wanninkhof, R., 1992. Relationship between wind speed and gas exchange over the ocean. J. Geophys. Res. 97 (C5), 7373–7382.

Williams, P.J.I., Robertson, J.E., 1991. Overall planktonic oxygen and carbon dioxide metabolisms: the problem of reconciling observations and calculations of photosynthetic quotients. Journal of plankton Research 13 (Supplement), 153–169.

Wong, G.T.F., 2012. Removal of nitrite interference in Winkler determination of dissolved oxygen in seawater. Mar. Chem. 130–131, 28–32.

Yin, K., Zhang, J., Qian, P.-Y., Jian, W., Huang, L., Chen, J., Wu, M.C.S., 2004. Effect of wind events on phytoplankton blooms in the Pearl River estuary during summer. Cont. Shelf Res. 24, 1909–1923.

Zhai, W., Dai, M., Cai, W.J., Wang, Y., Wang, Z., 2005. High partial pressure of $\mathrm{CO_2}$ and its maintaining mechanism in a subtropical estuary: the Pearl River estuary, China. Mar. Chem. 93 (1), 21–32.

Zhao, H.T., 1990. Evolution of the Pearl River Estuary. China Ocean Press, Beijing (357 pp., in Chinese).

Zhou, K., Dai, M., Kao, S.-J., Wang, L., Xiu, P., Chai, F., Tian, J., Liu, Y., 2013. Apparent enhancement of ^{234}Th-based particle export associated with anticyclonic eddies. Earth Planet. Sci. Lett. 381, 198–209.